PAPER

Catalytic activity of Pt$_{38}$ in the oxygen reduction reaction from first-principles simulations

Luca Sementa,[a] Oliviero Andreussi,[b]
William A. Goddard III[c] and Alessandro Fortunelli*[ac]

The activity of truncated octahedral Pt$_{38}$ clusters as a catalyst in the oxygen reduction reaction (ORR) is investigated *via* first-principles simulations. Three catalytic steps: O$_2$ dissociation (O$_{2ads}$ → 2O$_{ads}$), O hydration (O$_{ads}$ + H$_2$O$_{ads}$ → 2OH$_{ads}$), and H$_2$O formation (OH$_{ads}$ + H$_{ads}$ → H$_2$O$_{ads}$) are considered, in which all reactant species are co-adsorbed on the Pt$_{38}$ cluster according to a Langmuir–Hinshelwood mechanism. The minimum structures and saddle points for these different steps are then calculated at the density-functional theory (DFT) level using a gradient-corrected exchange–correlation (xc-)functional and taking into account the effect of the solvent *via* a self-consistent continuum solvation model. Moreover, first-principles molecular dynamics (AIMD) simulations in which the H$_2$O solvent is explicitly described are performed to explore dynamic phenomena such as fast hydrogen transfer *via* meta-stable hydronium-type configurations and their possible role in ORR reaction paths. By comparing the present findings with previous results on the Pt(111) surface, it is shown that in such a nanometer-size cluster the rate-determining-step (rds) corresponds to H$_2$O formation, at variance with the extended surface in which O hydration was rate-determining, and that the overall reaction barrier is actually increased with respect to the extended system. This is in agreement with and rationalizes experimental results showing a decrease of ORR catalytic activity in the nanometer-size cluster range.

Introduction

Among the challenges of present-day catalysis, those related to energy conversion are probably the most urgent ones.[1] Realizing a transformation from carbon-based to green energy production and storage is advocated as indispensable to prevent depletion of the earth fossil fuel reserves and the increase in green-house gas levels in the atmosphere.[2] In this context, hydrogen Fuel Cells (HFC), realizing hydrogen combustion and converting the chemical energy stored in this fuel into electrical energy, might play a crucial role.[3,4] Considerable efforts are thus being devoted world-wide to develop efficient HFC catalysts, overcoming the barrier represented by the inefficiency of the cathode oxygen reduction reaction (ORR), which is two orders of magnitude slower than the anode hydrogen oxidation reaction and represents a major obstacle to the development of a hydrogen economy. Until now, platinum-based catalysts achieve the top performance as ORR

catalysts, but the scarcity of this precious metal poses issues to its adoption in industrial mass-production.[5] Current research in this field is thus focused either on replacing Pt with non-precious alternatives or on reducing the needed amount of Pt *e.g.* in automotive converters.[6] Following the latter pathway, nanofabrication, *i.e.*, the use of nanometer-size particles, seems the most natural solution to increase the mass activity of precious catalysts, as the smaller the particles the larger the surface-to-volume ratio, and therefore the number of atoms potentially active in catalysis. However, numerous studies have shown that in the case of Pt-based systems their ORR activity has a peak for medium-size particles (around 5–8 nm in diameter) whereas small nanoparticles, especially those below 2 nm in diameter, are very poor catalysts.[7–9] Subnanometer clusters (or ultrananoclusters), *i.e.*, very small aggregates up to 10–20 metal atoms, represent an emergent subject,[10,11] but too few experimental studies have been conducted in the case of Pt/ORR and the picture in this extremely non-scalable régime still needs to be fully clarified.[12,13] In short, there is a lack of fundamental knowledge on the origins of the puzzling experimental observations on ORR activity of Pt-based systems, which hinders further progress in the field and their use in practical HFC devices. In addition to extensive experimental investigations, previous theoretical work has provided useful insight into the complex

[a] *CNR-ICCOM, Consiglio Nazionale delle Ricerche, via G. Moruzzi 1, I-56124 Pisa, Italy. E-mail: alessandro.fortunelli@cnr.it*
[b] *Inst. Computat. Sci., Univ. Svizzera Italiana, Via G. Buffi 13, CH-6904 Lugano, Switzerland*
[c] *Materials and Process Simulation Center, California Institute of Technology, 1200 E California Blvd, Pasadena, (CA) 91125, USA*

This journal is © The Royal Society of Chemistry 2016

Catal. Sci. Technol., 2016, **6**, 6901–6909 | 6901

problem of ORR kinetics on metal surfaces[14–23] but often focusing on extended systems or not addressing the issue of the crucial difference between these and small particles.[24]

Here we address this problem and try to understand the reasons for the decay of ORR activity in small Pt nanoparticles *via* first-principles modelling and simulations. We take a truncated-octahedral Pt_{38} aggregate as a realistic representative example of 1 nm clusters and as a system amenable to first-principles computations, and we conduct a systematic investigation using state-of-the-art density-functional theory (DFT) at both static and dynamic levels and with solvent effects described *via* both implicit and explicit (fully atomistic) models. As a result of this investigation, we single out too strong a binding of hydroxyl species to Pt_{38} (ultimately due to extreme under-coordination of surface atoms) as the main reason of high energy barrier in the ORR mechanism, specifically in the final step of the transformation of hydroxyls into water molecules (water formation). We then conclude by discussing possible ways to overcome this limitation and design ORR-effective nanometer-size Pt catalysts.

The article is organized as follows. In sec. 2 we give the details of the computational methods, sec. 3 presents results and discussion, while conclusions are summarized in sec. 4.
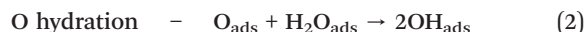
2. Computational details

Density-functional theory (DFT) calculations are performed using the plane-wave Quantum Espresso package.[25] The Perdew–Burke–Ernzerhof (PBE)[26] exchange–correlation functional is used together with ultrasoft pseudopotentials[27] and energy cutoffs of 40 Ry and 400 Ry for the wave function and electronic density, respectively. Structural optimizations and transition state searches are carried out in a spin-unrestricted formalism, with a cubic unit cell measuring 16 Å in side thus leaving at least 8 Å of empty space between atoms in replicated cells and the Brillouin zone sampled at the Gamma point only. In order to describe transition state energetics, reaction barriers are evaluated with a nudged elastic band (NEB)[28] transition state algorithm using the Climbing Image protocol with 7 intermediate images. It should be noted that some spin contamination is found in our DFT calculations, whose effect on reaction energy differences and energy barriers is however difficult to quantify. A continuum solvation model is used: the self-consistent continuum solvation model (SCCS) proposed by Andreussi, Dabo and Marzari,[29] and based on previous work by Fattebert *et al.*[30,31]

Ab initio molecular dynamics (AIMD) is performed using the CP2K code[32] whose DFT algorithms are based on a hybrid Gaussian/Plane-Wave scheme (GPW) developed by Lipper, Hutter and Parrinello.[33] We choose pseudopotentials derived by Goedecker, Teter and Hutter (GTH) to describe the core electrons[34] and DZVP basis sets[35] to represent the DFT Kohn–Sham orbitals. The energy cut-off for the auxiliary plane wave representation of the density is 300 Ry, while that for the representation of the wave function is 30 Ry. Each dynamics is followed for 1–4 ps with a time step of 1.5 fs during

which the temperature is controlled by Nosé–Hoover chain thermostats.[36] As in the Quantum Espresso calculations, the PBE functional is used.[26] The unit cell contains a Pt_{38} cluster, a total of 113 water molecule, plus 6 O and 6 H adatoms adsorbed on the metal cluster, in a cubic unit cell measuring 16 Å in side as in the implicit solvent calculations.

3. Results and discussion

In the following we focus on the following three steps of a Langmuir–Hinshelwood ORR mechanism:

$$O_2 \text{ dissociation} \quad - \quad O_{2ads} \rightarrow 2O_{ads} \quad (1)$$

$$O \text{ hydration} \quad - \quad O_{ads} + H_2O_{ads} \rightarrow 2OH_{ads} \quad (2)$$

$$H_2O \text{ formation} \quad - \quad OH_{ads} + H_{ads} \rightarrow H_2O_{ads} \quad (3)$$

These steps, that are pictorially illustrated in Fig. 1, 3 and 4, correspond to the following ORR path sequence:

• An O_2 molecule adsorbs on the Pt_{38} cluster and dissociates into two oxygen adatoms (O_{ads}) – O_2 dissociation, step (1)

• Adsorbed oxygen adatoms undergo a protonation step by reaction with an adsorbed water molecule (H_2O_{ads}) to give two adsorbed hydroxyl species (OH_{ads}) – O hydration, step (2)

• The last step is the protonation of an adsorbed hydroxyl to give an adsorbed water molecule – H_2O formation, step (3)

Focusing on a Langmuir–Hinshelwood mechanism (with all reactants adsorbed on the surface of the metal cluster) also for the H-species as done here implies that electron transfer processes are implicitly assumed to take place in the formation of H_{ads} species from a solvated H^+ species and an electron from the Pt cluster:

$$H_{ads} \text{ formation} - H_3O^+_{solv} + e^- \rightarrow H_2O_{solv} + H_{ads} \quad (4)$$
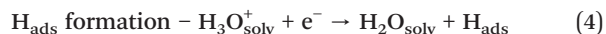
where $H_3O^+_{solv}$ and H_2O_{solv} are a solvated hydronium cation and a solvated water molecule, respectively. This choice of conditions corresponds to working at low electrochemical potential, in which Pt surfaces are covered with adsorbed
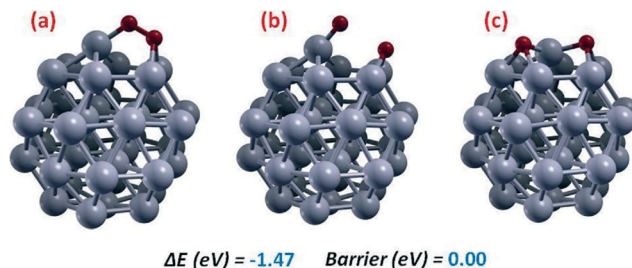

$\Delta E \ (eV) = -1.47$ $Barrier \ (eV) = 0.00$

Fig. 1 Pictorial illustration of the lowest-energy-barrier path and corresponding energetics for the dissociation of an O_2 molecule absorbed on Pt_{38}. (a, c) Initial and final local minima, respectively, and (b) saddle point. Platinum atoms as gray spheres, oxygen as red spheres, hydrogen as small white spheres.
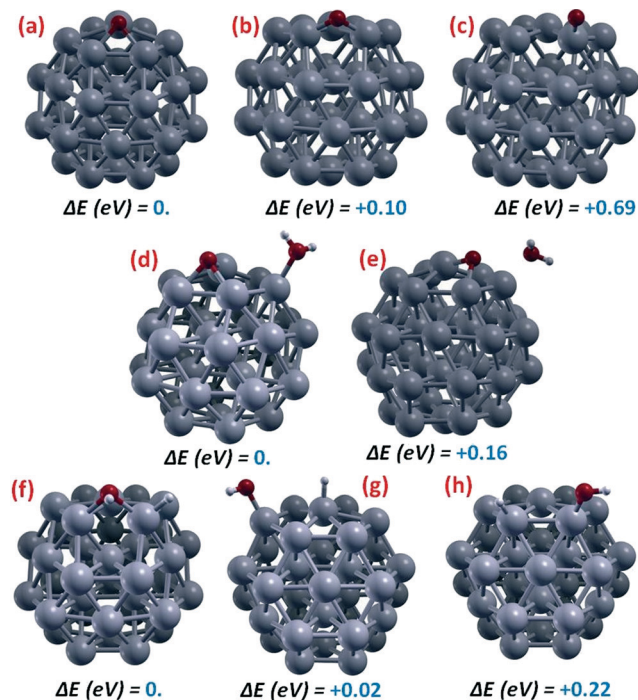
Fig. 2 Pictorial illustration of local minima configurations and corresponding relative energetics for the adsorption of ORR species on the Pt_{38} cluster: (a–c) oxygen adatom (O_{ads}); (d, e) co-adsorption of oxygen adatom and a water molecule ($O_{ads} + H_2O_{ads}$); (f–h) co-adsorption of a hydroxyl and a hydrogen atom ($OH_{ads} + H_{ads}$). Color coding as in Fig. 1.

Fig. 4 Pictorial illustration of the lowest-energy-barrier paths and corresponding energetics for OH-formation on Pt_{38}, starting from different initial structures: (a, c) initial and final local minima, respectively, and (b) saddle point starting from the structure of Fig. 2(f); (d, f) initial and final local minima, respectively, and (e) saddle point starting from the structure of Fig. 2(g); (g, i) initial and final local minima, respectively, and (h) saddle point starting from the structure of Fig. 2(h). Color coding as in Fig. 1.
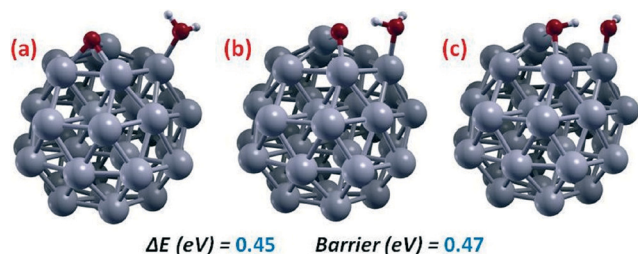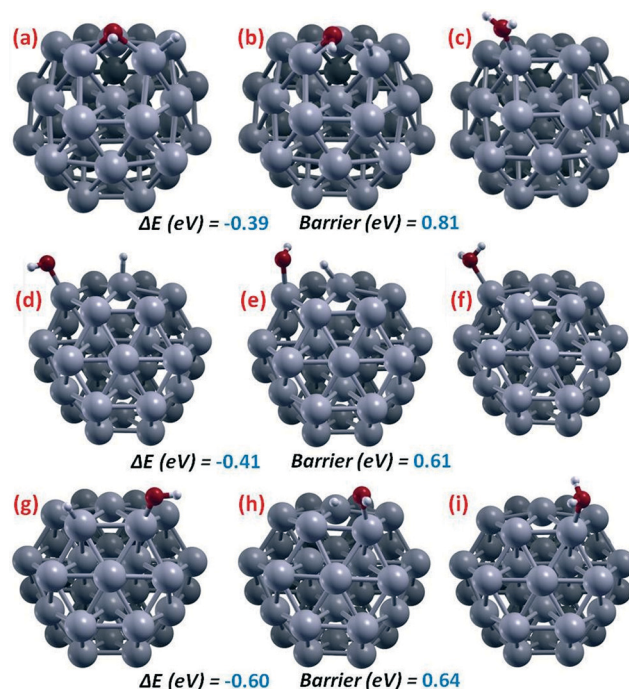

Fig. 3 Pictorial illustration of the lowest-energy-barrier path and corresponding energetics for O-hydration on Pt_{38}. (a, c) Initial and final local minima, respectively, and (b) saddle point. Color coding as in Fig. 1.

hydrogen atoms in acidic conditions.[37] This is the régime that has been extensively investigated in the computational literature on the Pt(111) catalyst surface,[14–24] thus allowing a direct comparison with extended Pt surfaces[38] and thus to understand the differences as ORR catalysts between the nanometer-size Pt_{38} cluster and a well characterized extended system.

Other mechanistic steps than (1–3) are possible and have been investigated in the literature. For example, paths going through H_2O_2 species, which however seem to be experimentally unfavorable on Pt catalysts.[39] Moreover – as we will see below – steps (1) and (2) have relatively low barriers on Pt_{38}, so that they cannot correspond to the rate-determining step (rds) of ORR. In short, we predict a fast transformation of O_2 into hydroxyls (OH_{ads}) *via* (1, 2) that can only be made faster by competitive paths.

Let us discuss our computational results. Our study will be divided into two parts:

(a) Implicit solvent simulations (section 3.a).

(b) Explicit solvent simulations (section 3.b).

The main body of this work, section 3.a, employs an implicit representation of the water solvent, allowing us to investigate in detail all the steps of the ORR. Additionally, selected simulations have also been conducted using a explicit representation of the water molecules surrounding the Pt_{38} cluster. These are intended to explore whether ORR proton-transfer mechanisms can occur by involving water molecules that formally do not take part to the given reaction step and that are thus only implicitly taken into account in a continuum (implicit) representation of the solvent. For example, such water molecules can act as shuttles for H species, and accelerate proton transfer processes, thus changing predicted energy barriers. These mechanism have been shown to play an important role in a variety of processes in aqueous media, see *e.g.* ref. 40 and 41, but to the best of our knowledge have not been considered so far in the context of ORR by Pt catalysts.

3.a Implicit solvent simulations

As a preliminary remark: all energies reported hereafter refer to full geometry optimization of local minima or saddle

points at the DFT/PBE+SCCS level, *i.e.*, always including the SCCS solvation contribution.

Fig. 1 shows the initial and final configurations and the connecting saddle point for O_2 dissociation, step (1). O_2 absorption is thermodynamically favored by 1.58 eV, and goes through a basically barrier-less process to produce two oxygen adatoms (O_{ads}), with an energy gain of −1.48 eV. This reaction has been thoroughly investigated on gas-phase Pt_{38} by Jennings *et al.*,[42] showing that the barrier is basically zero even in the absence of a solvent. This surprising result is at variance with the Pt(111) surface, in which the reaction barrier for O_2 dissociation in the gas-phase ranges around 0.5–0.6 eV,[19] and can be understood as due to the great structural flexibility of Pt_{38}, especially of the Pt atom at the center of the fcc(111)-like facet, which can easily protrude out of the facet. This structural flexibility has been previously discussed[43,44] and attributed to bonding directionality in 3rd-row transition metals (particularly Au and Pt) caused by the hybridization between 6s and 5d atomic functions in the valence band. Structural flexibility allows a strong adsorption of O_2 facilitating bond dissociation and enhances the interaction of the oxygen adatom with Pt_{38} – its adhesion energy in water is 5.09 eV *vs.* 4.43 eV on the Pt(111) surface, thus stabilizing the O_2-dissociation products and decreasing the corresponding energy barrier. On Pt(111) when water is added as a solvent the saddle-point of O_2 dissociation is substantially stabilized due to solvent polarization contributions, so that the dissociation barrier (that would otherwise be rate-determining) becomes negligible.[23] On Pt_{38}, the barrier is already negligible in the gas-phase, and solvent effects cannot further decrease it. This step is therefore both thermodynamically favored and kinetically extremely fast, and can be assumed to initiate the ORR mechanism.

Fig. 2 shows a sample of local minima configurations and corresponding relative energetics for the adsorption of ORR species on the Pt_{38} cluster: (a–c) oxygen adatom (O_{ads}); (d, e) co-adsorption of oxygen adatom and a water molecule (O_{ads} + H_2O_{ads}); (f–h) co-adsorption of a hydroxyl and a hydrogen atom (OH_{ads} + H_{ads}).

Starting from an oxygen adatom (O_{ads}) and taking the configuration resulting from O_2 dissociation in which the adsorption site is located on a fcc(111)-like facet, Fig. 2(a–c) show that adsorption in bridge sites between fcc(111)/fcc(100) facets and on-top of vertex Pt atoms are local minima in the solution phase (the presence of the solvent is necessary to transform these configuration from saddle points in the gas-phase to local minima in solution) but lie at higher energies. Especially the on-top position is unfavorable, with an energy difference of 0.69 eV with respect to the fcc(111)-facet adsorption, whereas the fcc(111)/fcc(100) bridge lies at only 0.1 eV higher in energy. Another local minimum (not shown in Fig. 2) is found in the 4-fold hollow site of the (100) facet, lying at 0.40 eV above the global minimum adsorption on fcc(111)-facet (the lowest-energy state for Pt_{38}–O). It may seem surprising that O-adsorption on the fcc(100) facet of Pt_{38} is actually less stable than on the fcc(111) facet (4.69 *vs.* 5.09

eV, respectively), since on extended surfaces the reverse is true, with fcc(100) adsorption stronger by 10% with respect to fcc(111) adsorption.[19] This is again due to the great structural freedom of the Pt atom at the center of the (111) facet, whereas a corresponding structural mechanism leading to enhancement of adsorption energy is not present for (100), demonstrating once more that ORR energetics is quite different on such small Pt clusters with respect to extended systems.

When a water molecule is added in Fig. 2(d and e), the O_{ads}-adsorption site does not change while H_2O adsorbs on-top of a vertex Pt atom – Fig. 2(d), but a fcc(111)/fcc(111) bridge position is also possible at an energy higher by only 0.16 eV, in which position however water is pushed away from the Pt cluster likely due to an unfavorable dipole–dipole repulsion together with the formation of an O_{ads}–H_2O_{ads} hydrogen bond – Fig. 2(e).

Finally, co-adsorption of a hydroxyl and a hydrogen is explored in Fig. 2(f–h): the global minimum is found to be with a hydroxyl on a fcc(111)/fcc(100) adsorption site and a hydrogen atom on a vertex Pt part of the bridge – Fig. 2(f) – but the hydroxyl can move on-top of a vertex Pt atoms while the hydrogen concurrently moves on-top of a Pt atom at the center of the fcc(111) facet with a negligible energy penalty (≈ 0.02 eV) – Fig. 2(g), whereas interestingly if the hydrogen is left on-top of a vertex Pt atom the energy difference is larger, 0.22 eV – Fig. 2(h).

Fig. 2(d and e) allows us to understand the mechanism of O_{ads}-protonation *via* O hydration, step (2), *i.e.*, reaction of O_{ads} with an adsorbed water molecule (H_2O_{ads}) to give two adsorbed hydroxyl species (OH_{ads}). The corresponding path is illustrated in Fig. 3. The energy barrier for this reaction is non-negligible, and is basically due to a positive reaction energy. Both the small difference between energy barrier and reaction energy and the substantial value of the reaction energy for O-hydration are due to the same physical effect: a large disfavorable solvation contribution, in analogy with the Pt(111) surface.[23] Indeed in the gas-phase we find much smaller values: $\Delta E = 0.07$ eV and Barrier = 0.19 eV for this reaction. The barrier for the O-hydration step is slightly higher but roughly comparable to the corresponding O-hydration on Pt(111), 0.40 eV, on which the O-hydration step was shown to be rate-determining.[19] We note in this connection that we have also sampled OH-formation *via* an (O_{ads} + H_{ads}) mechanism, but found it to have a much higher energy barrier (around 0.7 eV – see section 3.b), so that we do not report the corresponding results in detail.

The last ORR step is water formation, $OH_{ads} + H_{ads} \rightarrow H_2O_{ads}$ – step (3), whose results are illustrated in Fig. 4. Due to the fact that we found it to be rate-determining, this step has been analyzed in some detail, and all the three local minima configurations in Fig. 2(f–h) have been considered as initial structures for a saddle-point search. The energy barrier starting from the lowest-energy configuration, Fig. 2(f), has an energy barrier of 0.81 eV. A lower-barrier path is however found starting from the second lowest-energy configuration,

6904 | *Catal. Sci. Technol.*, 2016, **6**, 6901–6909

This journal is © The Royal Society of Chemistry 2016

Fig. 2(g), corresponding to a barrier of 0.61 eV, plus the energy penalty to reach this configuration, that is 0.02 eV, to produce a final barrier of 0.63 eV. It can be noted that the total barrier starting from the highest-energy configuration here investigated, Fig. 2(h), is 0.64 eV + 0.22 eV = 0.84 eV, thus representing the most unfavorable path for a Langmuir–Hinshelwood water formation on Pt_{38}.

Our conclusion is therefore that, at variance with the Pt(111) surface under identical conditions for which system the O-hydration step is rate-determining, *water formation is the ORR rds on Pt_{38}*: $OH_{ads} + H_{ads} \rightarrow H_2O_{ads}$ – step (3). Moreover the associated energy barrier of 0.63 eV is *larger* than the rds barrier on Pt(111), *i.e.*, the O-hydration step with a barrier of 0.40 eV. The increased strength of H and OH adsorption on Pt_{38} with respect to Pt(111) is responsible for this increase in the rds barrier: in the transition state of water formation the Pt–H and Pt–OH bonds must be partially broken, producing a high energy penalty and therefore a kinetic hindrance to the last step of ORR. Indeed, H adsorbs on a Pt_{38} vertex with a strength of 3.96 eV against 2.77 eV on Pt(111), while OH adsorbs on a fcc(111)/fcc(100) bridge site with 3.25 eV strength against 2.29 eV on Pt(111). A similar increased strength of O adsorption on Pt_{38} is responsible for the annihilation of the barrier to O_2 dissociation, the initial step of ORR, as recalled above, whereas the final ORR product, a water molecule, has an adsorption energy on Pt_{38} of 0.87 eV, also larger than on a Pt(111) surface, $\approx$0.4 eV. In a volcano-curve plot,[14] Pt_{38} thus lies on the side of the volcano with too large interaction with reactant species. This conclusion is in perfect tune with experimental results pointing to a decreased ORR activity of small Pt nanocluster, especially those with diameter smaller than 2 nm,[7–9] and thus helping to explain them.

3.b Explicit solvent simulations

The analysis in section 3.a has two main limitations: it is conducted at low ORR-coverage (corresponding to low values of the electrochemical potential) and assumes that the effect of the solvent can be described *via* a continuum SCCS model (implicit solvent). The first limitation is usually assumed in current literature, and allows us to make a direct comparison with it. The second limitation poses a more subtle question. Since hydrogen transfer processes are basic to ORR, one can wonder whether phenomena such as hydrogen tunneling, hopping, *etc.* involving water molecules that are not explicitly described by continuum solvation models might play a role. Indeed, these phenomena have been shown to influence sometimes decisively a variety of processes in aqueous media, see *e.g.* ref. 40 and 41.

To obtain some glimpse on this issue, we use a computationally more demanding *ab initio* molecular dynamics (AIMD) approach. We therefore built an explicitly solvated $Pt_{38}(O)_6(H)_6$ system consisting of a Pt_{38} cluster with 6 adsorbed O_{ads} and 6 adsorbed H_{ads} species and 113 surrounding water molecules sufficient to fill up a $16 \times 16 \times 16$ cubic box (see section 2 for more details). Moreover, since we did not observe any reactions in the time scale of our AIMD simulations when the O_{ads} were located in fcc(111) hollow sites, we moved them to positions on-top of vertex Pt atoms, to give the initial structure illustrated in Fig. 5. The analysis of these simulations provided us with a number of reaction and diffusion mechanisms, some of which are illustrated in Fig. 6–8.

First, we find that when the O_{ads} are moved from fcc(111) hollow sites to positions on-top of vertex Pt atoms, the O-hydration mechanism, $O_{ads} + H_2O_{ads} \rightarrow 2OH_{ads}$ – step (2), becomes extremely fast and is indeed immediately observed in our AIMD simulations. Two examples of such mechanisms are shown in the two stripes of Fig. 6, illustrating the same phenomenon: an O_{ads} adatom on top of a vertex Pt atom reacts with a water molecule adsorbed on a different vertex Pt atom. It can be observed that in the top stripe of Fig. 6 an intermediate water molecule acts as a shuttle of H-species *via* a mechanism in which: (a) a proton first hops from a water molecule adsorbed on the Pt cluster onto a water molecule in the solution phase to form a hydronium H_3O^+ transient species while simultaneously a H atom of another water molecule in the solution phase next to the so-formed hydronium cation starts hopping onto the O_{ads} adatom; (b) the hydronium cation releases a hydrogen to the neighboring water molecule while the H atom completes its path to the O_{ads} adatom transforming it into a hydroxyl. A less exotic O-hydration mechanism is illustrated in the bottom stripe of Fig. 6. Such processes are extremely fast: in less than 200 fs all the $6O_{ads}$ adatoms are transformed into OH_{ads} species. The energy barrier for such processes is basically the energy
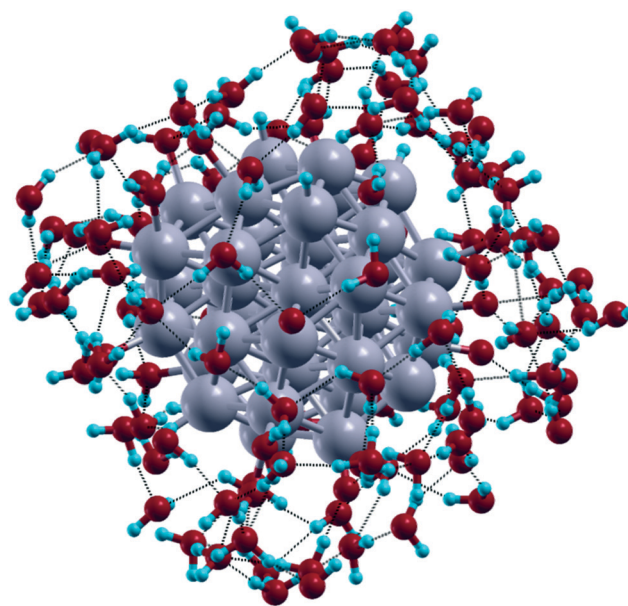

Fig. 5 Snapshot from AIMD simulations with the $Pt_{38}(O)_6(H)_6$ cluster used as initial structure with its first solvation shell of water molecules. Hydrogen bonds are highlighted by dotted lines and the outermost water molecules are omitted for clarity of illustration. Color coding as in Fig. 1, except that H atoms are light blue spheres.
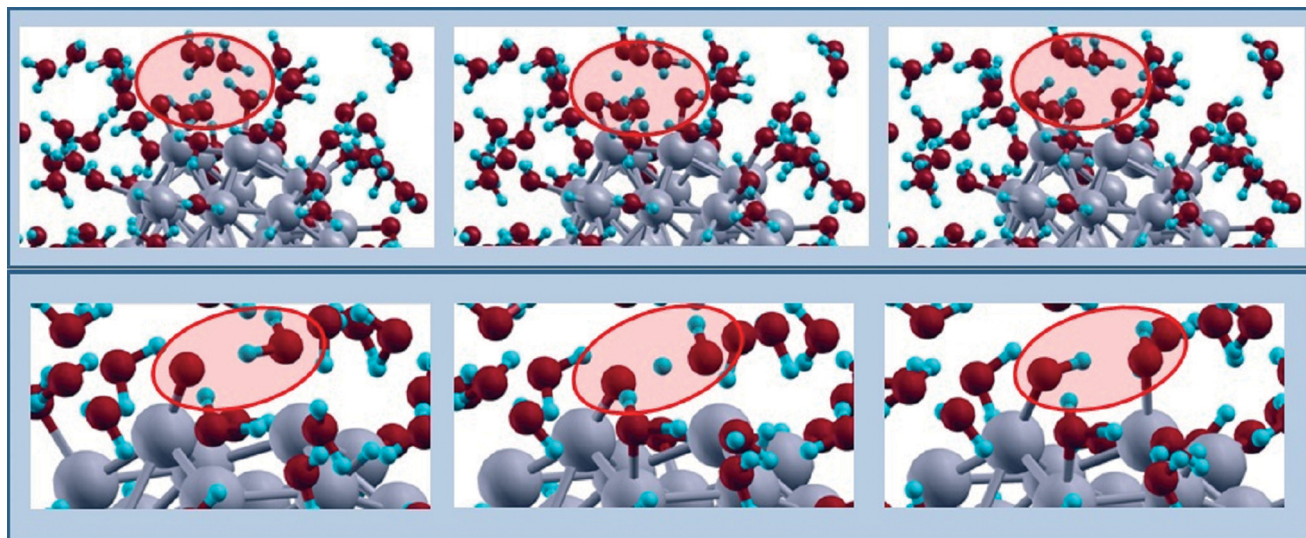
This journal is © The Royal Society of Chemistry 2016

Catal. Sci. Technol., 2016, **6**, 6901–6909 | **6905**

Fig. 6 Schematic illustration of two examples (top and bottom stripes, respectively) of O-hydration mechanisms occurring when O_{ads} adatoms on-top of vertex Pt react with a water molecule adsorbed on a different vertex Pt atom. In the top stripe an intermediate water molecule act as a shuttle of a H-species. Snapshots from AIMD simulations, red ovals highlighting the reactive regions. Color coding as in Fig. 5.
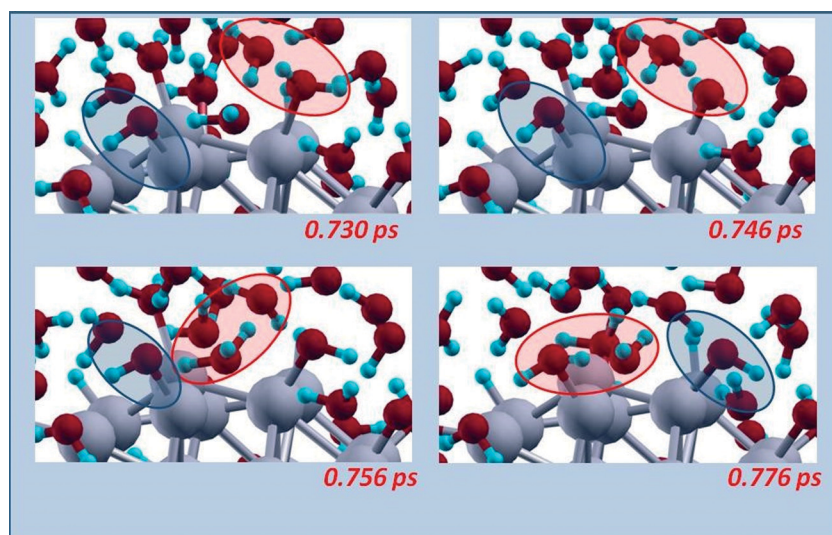

Fig. 7 Schematic illustration of a hydroxyl migration mechanisms occurring with an intermediate water molecule acting as a shuttle of a H-species. Snapshots from AIMD simulations, red and blue ovals highlighting the reactive regions. Color coding as in Fig. 5.
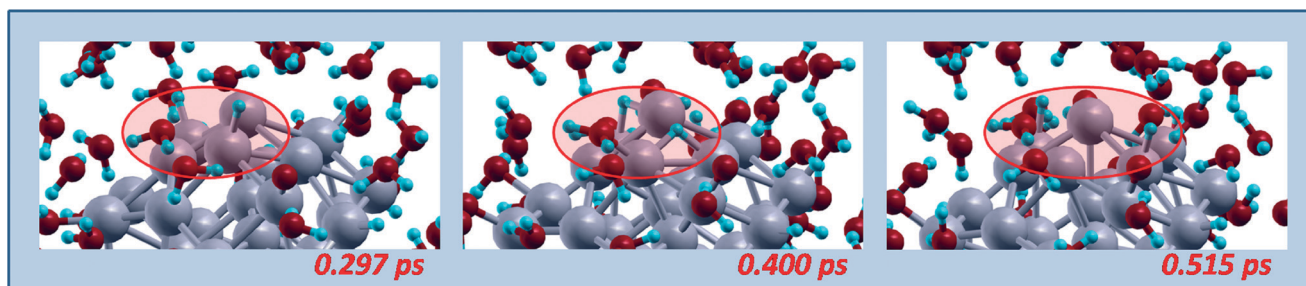

Fig. 8 Schematic illustration of a hydrogen diffusion mechanisms. Snapshots from AIMD simulations, red ovals highlighting the reactive regions. Color coding as in Fig. 5.

6906 | *Catal. Sci. Technol.*, 2016, **6**, 6901–6909

This journal is © The Royal Society of Chemistry 2016

to move a O_{ads} adatom from fcc(111) to on-top adsorption sites, *i.e.*, 0.69 eV from Fig. 2(c), and thus larger than the barrier for the path proposed in Fig. 3 as discussed above.

After these initial steps in which all the O_{ads} adatoms are transformed into OH_{ads} species, at later times other dynamic phenomena can be observed during the AIMD runs, such as in particular migration or diffusion processes. Fig. 7 illustrates a hydroxyl migration mechanism. Interestingly, this mechanism also occurs with an intermediate water molecule acting as a shuttle of a H-species and the formation of a H_3O^+ transient species. In particular, in a first stage a hydrogen atom jumps from an adsorbed water molecule (which thus turns into an adsorbed hydroxyl) to a neighboring water molecule to form a H_3O^+ transient species, which in a second stage transfers a proton to a neighboring water molecule which is thus transformed into a H_3O^+ transient species, which finally yields a proton to an adsorbed hydroxyl thus transforming it into an adsorbed water. Fig. 8 instead shows a hydrogen diffusion mechanism, in which adsorbed OH_{ads} jumps between on-top positions on two different vertex Pt atoms. It should be underlined that, in agreement with the large energy barriers predicted by our continuum solvation modeling in section 3.a, steps such as water formation, OH_{ads} + H_{ads} → H_2O_{ads} – step (3), or direct OH formation, O_{ads} + H_{ads} → OH_{ads}, starting from O_{ads} species adsorbed in hollow position of fcc(111) facets are *never* observed in our AIMD runs, implying that the corresponding energy barriers must be larger than at least 0.2–0.25 eV.

In short, we find that proton hopping mechanisms from one water to another and the formation of H_3O^+ hydronium transient species can occur and play a role in ORR catalysis, although in the present case they do not seem to be decisive in determining the overall rds of the reaction. It can be added that such mechanisms are to be expected in general terms, as they can be related to Grotthuss-like processes determining the anomalously high proton conductivity of water.[45]

Finally, we note that in this study we have not explored the possibility that water formation is achieved *via* protonation of the adsorbed hydroxyl (OH_{ads}) with a hydronium cation (H_3O^+) coming from the solution phase. We recall however that this possibility has been investigated in ref. 21 on the Pt(111) catalyst, finding that the energy profile of water formation is not dramatically altered when a hydronium cation rather than an adsorbed H atom is used as a reactant at reasonable values of the electrochemical potential, and we may expect that this is also the case on Pt_{38}. Further work will be needed to fully validate the present results.

4. Conclusions and perspectives

We have conducted a first-principles investigation of the energetics and reaction mechanisms of ORR on the Pt_{38} catalyst. Our main goal is to explain why small Pt nanoclusters are less ORR-active than larger ones (peak activity around 8 nm), especially the significant drop in activity for particles

below 2 nm in diameter, as found in the experiment.[7–9] In this investigation we use state-of-the-art DFT methods, with special attention to the important issue of solvent effects which are modelled according to two different procedures involving an implicit (continuum) or explicit (atomistic) description of the water solvent. Our results allow us to determine the rds of ORR on Pt_{38}, that is the reaction of adsorbed hydroxyls and hydrogen adatom to give a water molecule (water formation step), and its substantial energy barrier, definitively larger than that for ORR on the Pt(111) surface, and to single out a too strong adsorption of hydroxyls onto the cluster surface as the main issue for Pt_{38} to act as an ORR catalyst. This issue is ultimately connected with the under-coordinated character of surface atoms in such a small species: the consequent presence of fcc(111)/fcc(100) bridge adsorption sites favour binding of intermediate hydroxyls with respect to product water, thus increasing the energy barrier of the associated mechanistic step while annihilating the barrier of the initial O_2 dissociation step. Pt_{38} thus seems to be on the side of too strong adsorption of unsaturated intermediates in the ORR volcano-curve plot.[14] It should be noted that these features are expected to hold not only at low OH/O/H-coverage, *i.e.*, low electrochemical bias, as investigated in this work, but also when the Pt_{38} surface is covered with oxygenated species, as it is expected to occur at operating bias around 0.9 V, of interest for device applications. The present conclusions are thus expected to carry over to realistic ORR conditions. Finally, we recall that another possible issue in small Pt nanoclusters (below 100 atoms) that we have not investigated here is their tendency to amorphous or better surface-reconstructed icosahedral-like configurations,[44] in which however one can expect that the 5-fold coordination environment of surface atoms is unfavourable to ORR kinetics, as recently shown *via* first-principles simulations.[46] Here we have focused on a truncated-octahedral fcc-bulk-like structure that does not present this issue and is also a realistic model of larger ($\geq$100–200 atoms) Pt nanoparticles.

Having so clarified the atomistic origins of their ORR ineffectiveness, the question in perspective is whether and under which conditions small Pt clusters can be turned into better ORR catalysts, thus exploiting the dominant presence of surface atoms (32 over 38 in Pt_{38}, *i.e.*, 84%) potentially active in catalysis. We see two possible ways to answer this question.

First, systems could be devised that are nanostructured down to 1 nm dimensions and thus present high surface/volume ratios but in such a way to avoid the presence of excessively under-coordinated surface atoms and too strongly binding adsorption sites such as fcc(111)/fcc(100) bridge sites found on the surface of Pt_{38}. Highly anisotropic systems such as Pt nanowires represent a promising opportunity in this respect,[47,48] as the presence of only two nanometer-size dimensions could decrease the geometric curvature at the surface.

Second, it can be noted that solvation makes an appreciable contribution to the energy barrier of the water formation ORR step on Pt_{38}. Our SCCS method predicts in fact that the barrier for this ORR rds is 0.15 eV *smaller* in the gas phase

This journal is © The Royal Society of Chemistry 2016

Catal. Sci. Technol., 2016, **6**, 6901–6909 | **6907**

(in the absence of water solvent). It can therefore be hypothesized that, in analogy with extended Pt(111) surfaces,[23] ORR kinetics could be accelerated by tuning the dielectric constant of the solvent.

Work is in progress to explore these two possibilities.

Acknowledgements

References

1 L. N. Lewis, *Chem. Rev.*, 1993, **93**, 2693–2730.

2 X. Chen, C. Li, M. Gratzel, R. Kostecki and S. S. Mao, *Chem. Soc. Rev.*, 2012, **41**, 7909–7937.

3 N. Armaroli and V. Balzani, *ChemSusChem*, 2011, **4**, 21–36.

4 Fuel cells and hydrogen joint undertaking (FCH JU) Multi - Annual Work Plan 2014–2020, 30/06/2014.

5 P. Bihouix and B. de Guillebon, *Quel Futur pour les métaux? Raréfaction des métaux: un nouveau défi pour la société*, EDP Sciences, Les Ulis Cedex A, France, 2010.

6 M. K. Debe, *Nature*, 2012, **486**, 43–51.

7 J. Wu and H. Yang, *Acc. Chem. Res.*, 2013, **46**, 1848–1857.

8 G.-F. Wei and Z.-P. Liu, *Phys. Chem. Chem. Phys.*, 2013, **15**, 18555–18561.

9 S. E. F. Kleijn, S. C. S. Lai, M. T. M. Koper and P. R. Unwin, *Angew. Chem., Int. Ed.*, 2014, **53**, 3558–3586.

10 J. H. Sinfelt, *Acc. Chem. Res.*, 1987, **20**, 134–139.

11 E. C. Tyo and S. Vajda, *Nat. Nanotechnol.*, 2015, **10**, 577–588.

12 T. Imaoka, H. Kitazawa, W. J. Chun, S. Omura, K. Albrecht and K. Yamamoto, *J. Am. Chem. Soc.*, 2013, **135**, 13089–13095.

13 S. Proch, M. Wirth, H. S. White and S. L. Anderson, *J. Am. Chem. Soc.*, 2013, **135**, 3073–3086.

14 J. K. Norskov, J. Rossmeisl, A. Logadottir, L. Lindqvist, J. R. Kitchin, T. Bligaard and H. Jonsson, *J. Phys. Chem. B*, 2004, **108**, 17886–17892.

15 V. Rai, M. Aryanpour and H. Pitsch, *J. Phys. Chem. C*, 2008, **112**, 9760–9768.

16 A. U. Nikelar and M. Mavrikakis, *Surf. Sci.*, 2008, **602**, L89–L94.

17 J. Rossmeils and J. K. Norskov, *Surf. Sci.*, 2008, **602**, 2337–2338.

18 J. Greeley and J. K. Norskov, *J. Phys. Chem. C*, 2009, **113**, 4932–4939.

19 Y. Sha, T. H. Yu, B. V. Merinov, P. Shirvanian and W. A. Goddard, *J. Phys. Chem. Lett.*, 2011, **2**, 572–576.

20 Y. Sha, T. H. Yu, B. V. Merinov and W. A. Goddard, *J. Phys. Chem. C*, 2012, **116**, 6166–6173.

21 Y. Sha, T. H. Yu, B. V. Merinov, P. Shirvanian and W. A. Goddard, *J. Phys. Chem. C*, 2012, **116**, 21334–21342.

22 T. H. Yu, T. Hofman, Y. Sha, B. V. Merinov, D. J. Myers, C. Heske, P. Shirvanian and W. A. Goddard, *J. Phys. Chem. C*, 2013, **117**, 26598–26607.

23 A. Fortunelli, W. A. Goddard, Y. Sha, T. H. Yu, L. Sementa, G. Barcaro and O. Andreussi, *Angew. Chem., Int. Ed.*, 2014, **53**, 6669–6672.

24 J. A. Keith and T. Jacob, *Angew. Chem.*, 2010, **122**, 9711–9716.

25 P. Giannozzi, S. Baroni, N. Bonini, M. Calandra, R. Car, C. Cavazzoni, D. Ceresoli, G. Chiarotti, M. Cococcioni, I. Dabo, A. Dal Corso, S. De Gironcoli, S. Fabris, G. Fratesi, R. Gebauer, U. Gerstmann, C. Gougoussis, A. Kokalj, M. Lazzeri, L. Martin-Samos, N. Marzari, F. Mauri, R. Mazzarello, S. Paolini, A. Pasquarello, L. Paulatto, C. Sbraccia, S. Scandolo, G. Sclauzero, A. P. Seitsonen, A. Smogunov, P. Umari and R. M. Wentzcovitch, *J. Phys.: Condens. Matter*, 2009, **21**, 395502.

26 J. Perdew, K. Burke and M. Ernzerhof, *Phys. Rev. Lett.*, 1996, **77**, 3865–3868.

27 D. Vanderbilt, *Phys. Rev. B: Condens. Matter Mater. Phys.*, 1990, **41**, 7892–7895.

28 G. Henkelman, B. P. Uberuaga and H. Jonsson, *J. Chem. Phys.*, 2000, **113**, 9901–9904.

29 O. Andreussi, I. Dabo and N. Marzari, *J. Chem. Phys.*, 2012, **136**, 064102.

30 D. A. Scherlis, J. L. Fattebert, F. Gygi, M. Cococcioni and N. Marzari, *J. Chem. Phys.*, 2006, **124**, 074103.

31 J. L. Fattebert and F. Gygi, *J. Comput. Chem.*, 2002, **23**, 662–666.

32 J. Hutter, M. Iannuzzi, F. Schiffmann and J. VandeVondele, *WIREs Comput. Mol. Sci.*, 2014, **4**, 15–25.

33 G. Lippert, J. Hutter and M. Parrinello, *Theor. Chem. Acc.*, 1999, **103**, 124–140.

34 S. Goedecker, M. Teter and J. Hutter, *Phys. Rev. B: Condens. Matter Mater. Phys.*, 1996, **54**, 1703–1710.

35 J. VandeVondele and J. Hutter, *J. Chem. Phys.*, 2007, **127**, 114105.

36 G. Martyna, M. Klein and M. J. Tuckerman, *Chem. Phys.*, 1992, **97**, 2635–2643.

37 F. Eisert and A. Rosén, *Surf. Sci.*, 1997, **377–379**, 759–764.

38 T. Zhang and A. B. Anderson, *Electrochim. Acta*, 2007, **53**, 982–989.

39 C. M. Sanchez-Sanchez and A. J. Bard, *Anal. Chem.*, 2009, **81**, 8094–8100.

40 M. Ceriotti, J. Cuny, M. Parrinello and D. E. Manolopoulos, *Proc. Natl. Acad. Sci. U. S. A.*, 2013, **110**, 15591–15596.

41 Y. T. Law, S. Zafeiratos, S. G. Neophytides, A. Orfanidi, D. Costa, T. Dintzer, R. Arrigo, A. Knop-Gericke, R. Schlögl and E. R. Savinova, *Chem. Sci.*, 2015, **6**, 5635–5642.

42 P. C. Jennings, H. A. Aleksandrov, K. M. Neyman and R. L. Johnston, *Nanoscale*, 2014, **6**, 1153.

43 E. Aprà and A. Fortunelli, *J. Phys. Chem. A*, 2003, **107**, 2934–2942.

44 E. Aprà, F. Baletto, R. Ferrando and A. Fortunelli, *Phys. Rev. Lett.*, 2004, **93**, 065502.

45 O. Markovitch, H. Chen, S. Izvekov, F. Paesani, G. A. Voth and N. Agmon, *J. Phys. Chem. C*, 2008, **112**, 9456–9466.

6908 | *Catal. Sci. Technol.*, 2016, **6**, 6901–6909

This journal is © The Royal Society of Chemistry 2016

46 A. Fortunelli, W. A. Goddard, L. Sementa, G. Barcaro, F. R. Negreiros and A. Jaramillo-Botero, *Chem. Sci.*, 2015, **6**, 3915–3925.

47 C. Chen, Y. Kang, Z. Huo, Z. Zhu, W. Huang, H. L. Xin, J. D. Snyder, D. Li, J. A. Herron, M. Mavrikakis, M. Chi, K. L. More, Y. Li, N. M. Markovic, G. A. Somorjai, P. Yang and V. R. Stamenkovic, *Science*, 2014, **343**, 1339–1343.

48 H. J. Yin, S. L. Zhao, K. Zhao, A. Muqsit, H. J. Tang, L. Chang, H. J. Zhao, Y. Gao and Z. Y. Tang, *Nat. Commun.*, 2015, **6**, 6430.

This journal is © The Royal Society of Chemistry 2016

Catal. Sci. Technol., 2016, **6**, 6901–6909 | **6909**